Nonlinear Dyn (2020) 101:1397–1415
https://doi.org/10.1007/s11071-020-05812-2

ORIGINAL PAPER

Reproducing kernel Hilbert space embedding for adaptive estimation of nonlinearities in piezoelectric systems

Sai Tej Paruchuri · **Jia Guo** · **Andrew Kurdila**

Received: 15 February 2020 / Accepted: 7 July 2020 / Published online: 3 August 2020

Abstract Nonlinearities in piezoelectric systems can arise from internal factors such as nonlinear constitutive laws or external factors like realizations of boundary conditions. It can be difficult or even impossible to derive detailed models from the first principles of all the sources of nonlinearity in a system. This paper introduces adaptive estimator techniques to approximate the nonlinearities that can arise in certain classes of piezoelectric systems. Here an underlying structural assumption is that the nonlinearities can be modeled as continuous functions in a reproducing kernel Hilbert space (RKHS). This approach can be viewed as a data-driven method to approximate the unknown nonlinear system. This paper introduces the theory behind the adaptive estimator, discusses precise conditions that guarantee convergence of the function estimates, and studies the effectiveness of this approach numerically for a class of nonlinear piezoelectric composite beams.

Keywords Reproducing kernels · RKHS · Piezoelectric oscillators · Nonlinear oscillator · Data-driven modeling

S. T. Paruchuri (✉) · J. Guo · A. Kurdila
Department of Mechanical Engineering, Virginia Tech, Blacksburg, VA 24060, USA
e-mail: saitejp@vt.edu

J. Guo
e-mail: jguo18@vt.edu

A. Kurdila
e-mail: kurdila@vt.edu

1 Introduction

Researchers have studied piezoelectric systems extensively over the past three decades for applications to classical problems like vibration attenuation, which is described in general treatises like [1–4], as well as modern problems like energy harvesting [5,6]. Even though many of these studies model piezoelectric oscillators as linear systems, piezoelectric systems are often inherently nonlinear. At low input amplitudes, the effect of nonlinearity is ordinarily not very pronounced. However, linear models can fail to capture the dynamics of piezoelectric systems that undergo large displacements, velocities, accelerations, or electric field strengths. Researchers have consequently also developed nonlinear models for many examples of piezoelectric oscillators. A general account of nonlinear field theory as it arises in modeling piezoelectric continua can be found in Maugin [7], Yang [8,9], while reference [10] gives a good account of how active nonlinear piezostructural components are incorporated in typical plate or shell models.

Some of the models that are perhaps the most relevant to the system considered in this paper are [11–19]. In these studies, researchers investigate case-specific models that include higher-order polynomial terms in the constitutive laws. The models in the above publications by von Wagner and Hagedorn [11,12], von Wagner [13,14], Stanton et al. [15,16], Wolf and Gottlieb [17], Usher and Sim [18], Triplett and Quinn [19]

are representative of methods that include higher-order (polynomial) terms in the electric enthalpy density to construct nonlinear piezoelectric system models. Using the extended Hamilton's principle, Lagrange's equations, or Lagrange density methods then gives a corresponding set of nonlinear equations of motion. We can think of all of these methods, in general, as approximations of the constitutive laws in terms of power series expansions of the nonlinear term. These methods are powerful tools and have been successfully implemented to model nonlinearities in piezoelectric devices, as illustrated in the articles cited above. Such methods for studying nonlinear systems that make explicit use of power series approximations and polynomial classes of nonlinearities have a long history. A general discussion of the theory underlying these approaches for nonlinear systems can be found in well-known texts such as those by Guckenheimer and Holmes [20], Wiggins [21] for nonlinear systems theory, or Nayfeh [22] on perturbation methods. Much of the analysis carried out in using these methods relies expressly on knowing the exact form of the governing nonlinearity. When such knowledge is available, strong conclusions regarding the stability, the nature of bifurcations, the possibility of internal or parametric resonance, or even chaotic response of the system can often be made.

Nonlinearities in piezoelectric systems are not just limited to polynomials nonlinearities discussed above. There is a rich collection of the literature that studies history-dependent modeling in piezoelectric systems and can be broadly classified into (1) rate-dependent and (2) rate-independent methods. General accounts of the theory on history-dependent models can be found in Visintin [23], Brokate and Sprekels [24]. The former class of modeling approaches focuses on the relationship between the input control and output displacement. Examples of these methods include the Preisach model ([25–27]), Prandtl–Ishlinskii model ([28–31]), Krasnoselskii–Pokrovskii model ([32–34]), and Maxwell model ([35,36]). In the latter category of history-dependent models for piezoelectric systems, rate-dependent methods include the Bouc–Wen Hysteresis model ([37–39]), Dahl model ([40,41]), Duhem model ([42,43]). A review of all these methods can be found in Gan and Zhang [44]. Overall, it should be noted that the nature of history-dependent models in the above references varies substantially, much more so than the models that feature polynomial nonlinearities that appear in an ordinary differential equation. The equations governing history dependence in piezoelectrics may be cast in terms of functional differential equations, differential inclusions, or in terms of history-dependent operators depending on the reference.

The above methods are highly effective for modeling piezoelectric system behavior when we know the form of the underlying nonlinearities. However, it is not always easy to determine this knowledge with a high level of certainty. Even for the narrow class of polynomial nonlinearities in the electric enthalpy, the choice of which polynomial terms to include for a particular material at hand can be subtle. If the form of the polynomial nonlinearity is known, then the classical methods of attack such as in Guckenheimer and Holmes [20], Wiggins [21], and Nayfeh [22] can and should be applied: these approaches provide a framework for very strong conclusions. When a system at hand is poorly understood, or even unknown, data-driven identification methods have been developed to address such cases. To be sure, these techniques primarily focus on different types of conclusions than the methods that rely on precise knowledge of the form of the uncertainty. Data-driven estimation methods focus on conditions that ensure the convergence of a function estimate to the true unknown function, rate of convergence of the estimation error, and the study of types of uncertainties that can be estimated. Data-driven methods for linear systems are well-known, well-documented, and are described in classical texts like [45]. Some of these methods have been encoded in commercially available packages such as, for example, the LMS PolyMAX software. Data-driven modeling approaches developed explicitly for nonlinear systems are an area of increasing interest and as of yet to be fully developed. Researchers have used system identifications methods to estimate the parameters in the above class of conventional nonlinear modeling approaches discussed above Kao and Fung [46], Fung et al. [47], and Chen et al. [48]. On the other hand, data-driven approaches have also been used as standalone methods to model nonlinear system behavior. One example of such a technique is the Dynamic Mode Decomposition (DMD) method, which approximates Koopman modes to model the inherent dynamics [49–54]. Another example would be the use of machine learning methods to identify the underlying nonlinearities in piezoelectric systems [55–59].

In this paper, we introduce a novel data-driven approach for estimating nonlinearities in piezoelec-

tric systems. This approach is based on embedding the unknown nonlinear function appearing in the governing equation in a reproducing kernel Hilbert space (RKHS). The unknown function is subsequently estimated through adaptive parameter estimation. Identification methods that use RKHS have been studied for problems like terrain measurement [60], control of dynamical systems [61–63], sensor selection [64], and learning spatiotemporally evolving systems [65,66]. In this paper, we extend the methodology initially developed in Bobade et al. [60] to nonlinear piezoelectric systems, which are a type of nonautonomous system. The advantages are as follows:

1. Under some conditions, this technique provides a bound on the error between the actual and estimated unknown function.
2. There is a geometric interpretation of the error estimate, in terms of the positive limit set of the system equations, that describes the subset over which convergence is guaranteed. This is a newly observed property of the RKHS embedding method.
3. This technique not only gives us a nonlinear model but also estimates the underlying nonlinear function over a subspace of the state space.
4. Since the primary assumption is that the nonlinear function belongs to an RKHS, this technique can be implemented for a large class of nonlinearities.
5. Unlike conventional modeling techniques, the explicit structure of the uncertainty in the nonlinearity does not influence the estimation approach. If some portion of the nonlinearity is known, this knowledge can be used and only the unknown part of the nonlinearity needs to be estimated.

In this study, we take as a prototypical example of a piezoelectric system, a piezoelectric composite beam subject to base excitation, and we model its dynamics using an adaptive estimation technique based on the RKHS embedding method.

2 Nonlinear piezoelectric model

In this section, we derive the equations of motion of a piezoelectric bimorph beam as shown in Fig. 1. We assume that the beam is excited at its base by input z and the shunt circuit is open. The method given here represents the classical approach for deriving the governing equations for the target class of nonlinear piezoelectric composites. This section carefully describes the precise nature of some constitutive nonlinearities and reveals the limitations of the traditional linear models. In the current study, we have chosen the electric enthalpy density for nonlinear continua given in von Wagner and Hagedorn [11] to serve as the means to construct the governing equations and formulate the RKHS embedding approach. Note that the RKHS embedding techniques discussed in this paper are not limited to this problem and can be adapted to model other types of similar nonlinear electromechanical composite oscillators.

2.1 Nonlinear electric enthalpy density

The expression for electric enthalpy density for modeling linear piezoelectric continua is given by

$$\mathcal{H} = \frac{1}{2} C^E_{ijkl} S_{ij} S_{kl} - e_{mij} S_{ij} E_m - \frac{1}{2} \epsilon^S_{im} E_i E_m,$$

where C^E_{ijkl}, S_{ij}, e_{mij}, E_m, and ϵ^S_{im} are the Young's modulus, strain, piezoelectric coupling, electric field, and permittivity tensors, respectively. The quadratic form above is written using the summation convention. Based on thermodynamic considerations, the stress and electric displacement, T_{ij} and D_i, respectively, are defined in the relations

$$T_{ij} = \left.\frac{\partial \mathcal{H}}{\partial S_{ij}}\right|_{s,E}, \qquad -D_i = \left.\frac{\partial \mathcal{H}}{\partial E_i}\right|_{s,S}.$$

The associated constitutive laws of linear piezoelectricity have the form

$$\begin{Bmatrix} T_{ij} \\ D_m \end{Bmatrix} = \begin{bmatrix} C^E_{ijkl} & -e_{nij} \\ e_{mkl} & \epsilon^S_{mn} \end{bmatrix} \begin{Bmatrix} S_{kl} \\ E_n \end{Bmatrix},$$

where again the summation convention holds in the expression above. In the above equations, the superscripts on C^E_{ijkl} and ϵ^S_{mn} emphasize that these constants are measured when the electric field and strain are held constant. For piezoelectric beam bending models, consideration is restricted to constitutive laws that have the form

$$\begin{Bmatrix} T_x \\ D_z \end{Bmatrix} = \begin{bmatrix} C^E_{xx} & -e_{zx} \\ e_{zx} & \epsilon^S_{zz} \end{bmatrix} \begin{Bmatrix} S_x \\ E_z \end{Bmatrix},$$

where $x \sim 11$, $z \sim 3$ are the coordinate directions depicted in Fig. 1. The coordinate x is measured along the neutral axis that extends along the length of the beams, and z is in the transverse bending displacement direction. The permittivity at constant strain can be related to that at constant stress using the relation

$$\epsilon_{zz}^{S} = \epsilon_{zz}^{T} - d_{zx}^{2} C_{xx}^{E}.$$

The piezoelectric strain coefficient d_{zx} is related to the piezoelectric coupling constant e_{zx} by the equation $e_{zx} = C_{xx}^{E} d_{zx}$. The constitutive laws for the piezoelectric composite are

$$T_x = C_{xx}^{E} S_x - d_{zx} C_{xx}^{E} E_z,$$
$$D_z = d_{zx} C_{xx}^{E} S_x + (\epsilon_{zz}^{T} - d_{zx}^{2} C_{xx}^{E}) E_z.$$

A detailed discussion of this linear case can be found in Kurdila and Tarazaga [67], Tiersten [68] and Leo [3].

For large values of the field variables, the effects of nonlinearity in the piezoelectric continua can become dominant. We account for these effects by adding higher-order terms in the expression for the electric enthalpy density. The nonlinear dependence between C_{xx}^{E}, d_{zx} and S_x can be approximated using the relations [11]

$$C_{xx}^{E} = C_{xx}^{E(0)} + C_{xx}^{E(1)} S_x + C_{xx}^{E(2)} S_x^2,$$
$$d_{zx} = d_{zx}^{(0)} + d_{zx}^{(1)} S_x + d_{zx}^{(2)} S_x^2.$$

The corresponding electric enthalpy density has the form

$$\mathcal{H} = \frac{1}{2} C_{xx}^{E(0)} S_x^2 + \frac{1}{3} C_{xx}^{E(1)} S_x^3 + \frac{1}{4} C_{xx}^{E(2)} S_x^4 - \gamma_0 S_x E - \frac{1}{2} \gamma_1 S_x^2 E - \frac{1}{2} \nu_0 E^2 \quad (1)$$

with

$$\nu_0 = \epsilon^{T} - (d_{zx}^{(0)})^2 C_{xx}^{E(0)},$$
$$\gamma_0 = C_{xx}^{E(0)} d_{zx}^{(0)},$$
$$\gamma_1 = C_{xx}^{E(0)} d_{zx}^{(1)} + C_{xx}^{E(1)} d_{zx}^{(0)},$$
$$\gamma_2 = C_{xx}^{E(0)} d_{zx}^{(2)} + C_{xx}^{E(2)} d_{zx}^{(0)} + C_{xx}^{E(1)} d_{zx}^{(1)}.$$

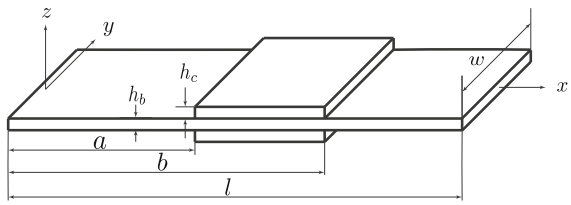

Fig. 1 Function 2D plot

Thus, the nonlinear constitutive laws, obtained using the relations shown above, have the form

$$T_x = C_{xx}^{E(0)} S_x + C_{xx}^{E(1)} S_x^2 + C_{xx}^{E(2)} S_x^3 - \gamma_0 E_z - \gamma_1 S_x E_z - \gamma_2 S_x^2 E_z,$$
$$D_z = \gamma_0 S_x + \frac{1}{2} \gamma_1 S_x^2 + \frac{1}{3} \gamma_2 S_x^3 + \nu_0 E_z.$$

See references [15,16,69–71] for other similar models that are used to represent the behavior of nonlinear piezoelectric systems.

2.2 Equations of motion

In this subsection, we derive the nonlinear equations of motion of the typical piezoelectric composite, the cantilevered bimorph, as shown in Fig. 1. The extended Hamilton's Principle states that of all the possible trajectories in the electromechanical configuration space, the actual motion satisfies the variational identity

$$\delta \int_{t_0}^{t_1} (T - \mathcal{V}_{\mathcal{H}})\, \mathrm{d}t + \int_{t_0}^{t_1} \delta W \mathrm{d}t = 0 \quad (2)$$

with kinetic energy T, electromechanical potential $\mathcal{V}_{\mathcal{H}}$ defined below, electromechanical virtual work δW, initial time t_0, and final time t_1. The kinetic energy of the nonlinear piezoelectric beam is expressed as

$$T = \frac{1}{2} \int_0^l m(x)(\dot{w} + \dot{\mathrm{z}})^2 dx = \frac{1}{2} \mathrm{m} \int_0^l (\dot{w} + \dot{\mathrm{z}})^2 dx \quad (3)$$

with $m(x)$ the mass per unit length of the beam and m defined as $\mathrm{m} = \rho_s h_s + 2\rho_p h_p$. In the above equation, $w = w(x, t)$ is the displacement from the neutral axis at location $x \in [0, l]$ at time t. The variable $\mathrm{z}(t)$ represents the displacement of the root of the beam,

that is, it is the base motion that occurs in the z direction defined relative to the beam. The terms ρ and h represent the density and thickness, respectively. The subscript s represents the variables corresponding to the substrate and the subscript p indicates those of the piezoceramic. The electric enthalpy for the nonlinear system is given by the relation

$$\mathcal{V}_{\mathcal{H}} = \int_V \mathcal{H}\mathrm{d}V = \int_{V_b} \mathcal{H}\mathrm{d}V_b + \int_{V_p} \mathcal{H}\mathrm{d}V_p.$$

Substituting the expression for $\mathcal{H}$ in the above equation gives

$$\begin{aligned}\mathcal{V}_{\mathcal{H}} = &\int_{V_b} \frac{1}{2}C_b S_x^2 \mathrm{d}V_b + \int_{V_c} \left(\frac{1}{2}C_{xx}^{(0)} S_x^2 \right.\\ &+ \frac{1}{3}C_{xx}^{(1)} S_x^3 + \frac{1}{4}C_{xx}^{(2)} S_x^4 - \gamma_0 S_x E_z\\ &\left. - \frac{1}{2}\gamma_1 S_x^2 E_z - \frac{1}{3}\gamma_2 S_x^3 E_z - \frac{1}{2}\nu_0 E_z^2\right)\mathrm{d}V_p \end{aligned} \tag{4}$$

with beam Young's modulus C_b, beam volume V_b and piezoelectric patch volume V_p. We recall that the approximation for bending strain in Euler–Bernoulli beam theory is given by

$$S_x(x,z,t) = -\frac{\partial^2 w(x,t)}{\partial x^2} z,$$

$\forall x \in [0,l], \quad \forall z \in \left[-\frac{h_b}{2} - h_c, \frac{h_b}{2} + h_c\right]$. Consider the term $\int_{V_p} \frac{1}{2}C_{xx}^{(0)} S_x^2$ in the expression for electric enthalpy density. With the substitution of the expression for strain, we get

$$\begin{aligned}&\int_{V_p} \frac{1}{2}C_{xx}^{(0)} S_x^2 = \frac{1}{2}C_{xx}^{(0)} \int_{V_p} [(w'')^2 z^2]\mathrm{d}V\\ &= \frac{1}{2}C_{xx}^{(0)} \left(\int_a^b (w'')^2 \mathrm{d}x\right)\left(\int_0^b \mathrm{d}y\right)\left(2\int_{\frac{h_b}{2}}^{\frac{h_b}{2}+h_c} z^2 \mathrm{d}z\right)\\ &= 2\underbrace{\left[\frac{1}{6}C_{xx}^{(0)} b\left\{\left(\frac{h_b}{2}+h_c\right)^3 - \left(\frac{h_b}{2}\right)^3\right\}\right]}_{:=a_{(0,2)}} \int_a^b (w'')^2 \mathrm{d}x\\ &= 2a_{(0,2)} \int_a^b (w'')^2 \mathrm{d}x. \end{aligned}$$

The other terms in Eq. 4 can be simplified in a similar manner. The expression for electric enthalpy density after simplification has the form

$$\begin{aligned}\mathcal{V}_{\mathcal{H}} = &\frac{1}{2}C_b I_b \int_0^l (w'')^2 \mathrm{d}x\\ &+ 2a_{(0,2)} \int_a^b (w'')^2 \mathrm{d}x + 2a_{(2,4)} \int_a^b (w'')^4 \mathrm{d}x\\ &+ 2b_{(1,1)} \left(\int_a^b w'' \mathrm{d}x\right) E_z\\ &+ 2b_{(3,1)} \left(\int_a^b (w'')^3 \mathrm{d}x\right) E_z - 2b_{(0,2)} E_z^2, \end{aligned} \tag{5}$$

where we define

$$\begin{aligned} a_{(0,2)} &:= \frac{1}{6}C_{xx}^{(0)} b\left[\left(\frac{h_b}{2}+h_c\right)^3 - \left(\frac{h_b}{2}\right)^3\right],\\ a_{(2,4)} &:= \frac{1}{20}C_{xx}^{(2)} b\left[\left(\frac{h_b}{2}+h_c\right)^5 - \left(\frac{h_b}{2}\right)^5\right],\\ b_{(0,2)} &:= \frac{1}{2}\nu_0 b h_c l_c,\\ b_{(1,1)} &:= \frac{1}{2}\gamma_0 b\left[\left(\frac{h_b}{2}+h_c\right)^2 - \left(\frac{h_b}{2}\right)^2\right],\\ b_{(3,1)} &:= \frac{1}{12}\gamma_2 b\left[\left(\frac{h_b}{2}+h_c\right)^4 - \left(\frac{h_b}{2}\right)^4\right]. \end{aligned}$$

For the time being, we omit the effects of damping in the following derivation. Following the details included in "Appendix A", the variational statement of Hamilton's principle yields the pair of equations

$$\begin{aligned}&\mathrm{m}\ddot{w} + C_b I_b w'''' + 4a_{(0,2)}\left(\chi_{[a,b]} w''\right)''\\ &\quad + 8a_{(2,4)}(\chi_{[a,b]}(w'')^3)'' + 2b_{(1,1)}\chi''_{[a,b]} E_z\\ &\quad + 6b_{(3,1)}(\chi_{[a,b]}(w'')^2)'' E_z = -\mathrm{m}\ddot{z}, \end{aligned} \tag{6}$$

$$\begin{aligned}&2b_{(1,1)} w'(b) - 2b_{(1,1)} w'(a)\\ &\quad + 2b_{(3,1)}\left(\int_a^b (w'')^3 \mathrm{d}x\right) + 4b_{(0,2)} E_z = 0, \end{aligned} \tag{7}$$

where $\chi_{[a,b]}$ is the characteristic function of the interval $[a,b]$ defined as in Eq. 23. These equations are subject to the corresponding variational boundary conditions

$$\begin{aligned}&\left\{C_b I_b w'' + 4a_{(0,2)}\chi_{[a,b]} w'' + 8a_{(2,4)}\chi_{[a,b]}(w'')^3\right.\\ &\quad \left. + 2b_{(1,1)}\chi_{[a,b]} E_z + 6b_{(3,1)}\chi_{[a,b]}(w'')^2\right\}\delta w'\Big|_0^l = 0, \end{aligned}$$

$$\Big\{C_b I_b w''' + 4a_{(0,2)}\left(\chi_{[a,b]}w''\right)' + 8a_{(2,4)}\left(\chi_{[a,b]}(w'')^3\right)' + 2b_{(1,1)}\chi'_{[a,b]}E_z + 6b_{(3,1)}\left(\chi_{[a,b]}(w'')^2\right)'\Big\}\delta w\Big|_0^l = 0,$$

and to the initial conditions $w(0) = w_0$ and $\dot{w}(0) = \dot{w}_0$.

We know that the effects of nonlinearity in oscillators become most noticeable near the natural frequency. Hence, we approximate the solutions of Eqs. 6 and 7 using a single-mode approximation $w(x,t) = \psi(x)u(t)$. Following the detailed analysis in "Appendix B", the equations of motion are written

$$M\ddot{u}(t) + P\ddot{z}(t) + \underbrace{[K_b + K_p]}_{K}u(t) + K_N u^3(t) + [\mathcal{B} + Q_N u^2(t)]E_z = 0, \quad (8)$$

$$\mathcal{B}u(t) + \mathcal{B}_N u^3(t) = \mathcal{C}E_z \quad (9)$$

for constants M, P, K_b, K_p, K_N, $\mathcal{B}$, Q_N, $\mathcal{B}_N$, and $\mathcal{C}$ defined in "Appendix B".

Note that the first equation defines the dynamics of the system and the second equation defines an algebraic relation between displacement and the electric field. From the second equation of motion, we get an expression for the electric field that has the form $E_z = [\mathcal{B}u(t) + \mathcal{B}_N u^3(t)]/\mathcal{C}$. Substituting this expression for electric field into the first equation of motion, we get

$$-P\ddot{z}(t) = M\ddot{u}(t) + \underbrace{\left[K + \frac{\mathcal{B}^2}{\mathcal{C}}\right]}_{\hat{K}}u(t) + \underbrace{\left[K_N + \frac{\mathcal{B}\mathcal{B}_N}{\mathcal{C}} + \frac{Q_N\mathcal{B}}{\mathcal{C}}\right]}_{\hat{K}_{N_1}}u^3(t) + \underbrace{\frac{Q_N\mathcal{B}_N}{\mathcal{C}}}_{\hat{K}_{N_2}}u^5(t),$$

$$-P\ddot{z}(t) = M\ddot{u}(t) + \hat{K}u(t) + \hat{K}_{N_1}u^3(t) + \hat{K}_{N_2}u^5(t).$$

After introducing a viscous damping term for the representation of energy losses, we have

$$M\ddot{u}(t) + C\dot{u}(t) + \hat{K}u(t) + \hat{K}_{N_1}u^3(t) + \hat{K}_{N_2}u^5(t) = -P\ddot{z}(t).$$

Let us define the state vector $\boldsymbol{x} = \{x_1, x_2\}^T = \{u, \dot{u}\}^T$. Now, we can write the first-order form of the governing equations as

$$\begin{Bmatrix}\dot{x}_1\\ \dot{x}_2\end{Bmatrix} = \underbrace{\begin{bmatrix}0 & 1\\ -\frac{\hat{K}}{M} & -\frac{C}{M}\end{bmatrix}}_{A}\begin{Bmatrix}x_1\\ x_2\end{Bmatrix} + \underbrace{\begin{Bmatrix}0\\ -\frac{P}{M}\end{Bmatrix}}_{B}\underbrace{\ddot{z}(t)}_{\mathrm{u}(t)} + \underbrace{\begin{Bmatrix}0\\ 1\end{Bmatrix}}_{B_N}\underbrace{\left(-\frac{\hat{K}_{N_1}}{M}x_1^3(t) - \frac{\hat{K}_{N_2}}{M}x_1^5(t)\right)}_{f(\boldsymbol{x}(t))}, \quad (10)$$

or

$$\dot{\boldsymbol{x}}(t) = A\boldsymbol{x}(t) + B\mathrm{u}(t) + B_N f(\boldsymbol{x}(t)).$$

We make several observations before proceeding to the adaptive estimation problem treated in the next section. Note that the specific form of function $f(\boldsymbol{x}) = f(x_1)$ that is given in Eq. 10 has been constructed assuming the only unknown terms are the nonlinearities arising from the constitutive laws. We allow for a wider class of uncertainty that can be expressed as $f(\boldsymbol{x}) = f(x_1, x_2)$. For instance, if the viscous damping coefficient is uncertain or unknown, the damping term should be subsumed into $f(x_1, x_2)$. With these considerations in mind, the derivations in the next section are carried out for the more general case when $f = f(x_1, x_2)$. However, when we prepare finite-dimensional approximations in Sect. 3.2 for the simulations in Sects. 4 and 5 , we specialize examples to the case $f = f(x_1)$ described above.

3 Adaptive estimation in RKHS

In this section, we pose the estimation problem for the approximation of the unknown nonlinear function f and review the theory of RKHS adaptive estimation. The governing equation of the plant, the piezoelectric oscillator modeled in Sect. 2, has the general form

$$\dot{\boldsymbol{x}}(t) = A\boldsymbol{x}(t) + B\mathrm{u}(t) + B_N f(\boldsymbol{x}(t)). \quad (11)$$

We denote the state space of this evolution law by $X = \mathbb{R}^d$, so that $\boldsymbol{x}(t) \in X$. Under the assumption of full state observability, the problem of estimation of the states $\boldsymbol{x}(t)$ at a given time instant t is a classical state estimation problem. However, the problem of interest in this paper is the estimation of the unknown function f. Problems of this type generally involve the definition of an estimator system that evolves in parallel with the

actual plant. The model of the estimator for the plant defined by Eq. 11 is taken in the form

$$\dot{\hat{\boldsymbol{x}}}(t) = A\hat{\boldsymbol{x}}(t) + B\mathrm{u}(t) + B_N \hat{f}(t, \boldsymbol{x}(t)). \tag{12}$$

In Eq. 12, note that the estimate $\hat{f}$ of the function f depends not only on the actual (measured) states $\boldsymbol{x}(t)$ but also the time t. We want the function estimate $\hat{f}(t, \cdot)$ to converge in time to the actual function $f(\cdot)$ in some suitable function space norm as $t \to \infty$.

In addition to the estimator model, it is also important to define the hypothesis space, the space of functions in which the function f and the function estimate $\hat{f}$ live. In this paper, we assume that the unknown nonlinear function f lives in the infinite-dimensional RKHS $\mathcal{H}_X$ equipped with the reproducing kernel $\mathcal{K}_X : X \times X \to \mathbb{R}$. Recall that the reproducing property of the kernel states that, for any $\boldsymbol{x} \in X$ and $f \in \mathcal{H}_X$, $(\mathcal{K}(\boldsymbol{x}, \cdot), f)_{\mathcal{H}_X} = f(\boldsymbol{x})$. It is well known that the existence of a reproducing kernel guarantees the boundedness of the evaluation functional $\mathcal{E}_{\boldsymbol{x}} : \mathcal{H}_X \to \mathbb{R}$, which is defined by the condition that $\mathcal{E}_{\boldsymbol{x}} f = (\mathcal{K}(\boldsymbol{x}, \cdot), f)_{\mathcal{H}_X}$. In this paper, we restrict to RKHS in which the reproducing kernel is bounded by a constant. This implies that the injection $i : \mathcal{H}_X \to C(\Omega)$ from the RKHS $\mathcal{H}_X$ to the space of continuous function on Ω, $C(\Omega)$, is uniformly bounded [60]. This fact is used to prove the existence and uniqueness of the solution of the error system. A more detailed discussion about RKHS can be found in Aronszajn [72], Berlinet and Thomas-Agnan [73], Muandet et al. [74].

In addition to the estimator model, we also need an equation that defines the evolution (time derivative) of the function estimate. This is given by the learning law

$$\dot{\hat{f}}(t) = \Gamma^{-1}(B_N \mathcal{E}_{\boldsymbol{x}(t)})^* P(\boldsymbol{x}(t) - \hat{\boldsymbol{x}}(t)), \tag{13}$$

where $\Gamma \in \mathbb{R}^+$, $\mathcal{E}_{\boldsymbol{x}}$ is the evaluation functional at $\boldsymbol{x} \in X$, and the notation $(\cdot)^*$ denotes the adjoint of an operator. Further, the matrix $P \in \mathbb{R}^{d\times d}$ is the symmetric positive definite solution of the Lyapunov's equation $A^T P + PA = -Q$, where $Q \in \mathbb{R}^{d\times d}$ is an arbitrary but fixed symmetric positive definite matrix.

The existence and uniqueness of a solution for the estimator models given by Eqs. 12 and 13 can be proved under the assumption that the excitation input is continuous and we are working in an uniformly embedded RKHS as mentioned above. The following theorem proves this statement.

Theorem 1 *Define* $\mathbb{X} := \mathbb{R}^d \times \mathcal{H}_X$, *and suppose that* $\boldsymbol{x} \in C([0, T]; \mathbb{R}^d)$, $\mathrm{u} \in C([0, T]; \mathbb{R})$ *and that the embedding* $i : \mathcal{H}_X \hookrightarrow C(\Omega)$ *is uniform in the sense that there is a constant* $C > 0$ *such that for any* $f \in \mathcal{H}_X$,

$$\|f\|_{C(\Omega)} \equiv \|if\|_{C(\Omega)} \le C\|f\|_{\mathcal{H}_X}.$$

Then for any $T > 0$, *there is a unique mild solution* $(\hat{\boldsymbol{x}}, \hat{f}) \in C([0, T], \mathbb{X})$ *to*

$$\begin{Bmatrix} \dot{\hat{\boldsymbol{x}}}(t) \\ \dot{\hat{f}}(t) \end{Bmatrix} = \begin{Bmatrix} A\hat{\boldsymbol{x}}(t) + B\mathrm{u}(t) + B_N \mathcal{E}_{\boldsymbol{x}(t)} \hat{f}(t) \\ \Gamma^{-1}(B_N \mathcal{E}_{\boldsymbol{x}(t)})^* P(\boldsymbol{x}(t) - \hat{\boldsymbol{x}}(t)) \end{Bmatrix}, \tag{14}$$

and the map $\hat{X}_0 \equiv (\hat{\boldsymbol{x}}_0, \hat{f}_0) \mapsto (\hat{\boldsymbol{x}}, \hat{f})$ *is Lipschitz continuous from* $\mathbb{X}$ *to* $C([0, T], \mathbb{X})$.

Proof We set $X(t) := (\hat{x}(t), \hat{f}(t)) \in \mathbb{X}$. Equation 14 can be rewritten as

$$\begin{Bmatrix} \dot{\hat{\boldsymbol{x}}}(t) \\ \dot{\hat{f}}(t) \end{Bmatrix} = \underbrace{\begin{bmatrix} A & 0 \\ 0 & A_0 \end{bmatrix}}_{\mathcal{A}} \begin{Bmatrix} \hat{\boldsymbol{x}}(t) \\ \hat{f}(t) \end{Bmatrix} + \underbrace{\begin{Bmatrix} B\mathrm{u}(t) + B_N \mathcal{E}_{\boldsymbol{x}(t)} \hat{f}(t) \\ -A_0 \hat{f}(t) + \Gamma^{-1}(B_N \mathcal{E}_{\boldsymbol{x}(t)})^* P(\boldsymbol{x}(t) - \hat{\boldsymbol{x}}(t)) \end{Bmatrix}}_{\mathcal{F}(t, X(t))},$$

$$\begin{Bmatrix} \hat{\boldsymbol{x}}(t_0) \\ \hat{f}(t_0) \end{Bmatrix} = \begin{Bmatrix} \hat{\boldsymbol{x}}_0 \\ \hat{f}_0 \end{Bmatrix}, \tag{15}$$

where $-A_0$ is an arbitrary bounded linear operator from $\mathcal{H}_X$ to $\mathcal{H}_X$. It is clear from the above equation that $\mathcal{A}$ is a bounded linear operator. We know that every bounded linear operator is the infinitesimal generator of a C_0-semigroup on $\mathbb{X} := \mathbb{R}^d \times \mathcal{H}_X$ (Theorem 1.2, Chapter 1 of Pazy [75]). Now, consider the function $\mathcal{F}$. For each $t \ge 0$, we have

$$\begin{aligned} &\|\mathcal{F}(t, \hat{X}) - \mathcal{F}(t, \hat{Y})\| \\ &= \left\| \begin{Bmatrix} B_N \mathcal{E}_{\boldsymbol{x}(t)} (\hat{f}_{\hat{x}}(t) - \hat{f}_{\hat{y}}(t)) \\ -A_0 (\hat{f}_{\hat{x}}(t) - \hat{f}_{\hat{y}}(t)) + \Gamma^{-1} (B_N \mathcal{E}_{\boldsymbol{x}(t)})^* P(\hat{y}(t) - \hat{x}(t)) \end{Bmatrix} \right\| \\ &\le D\|\hat{X} - \hat{Y}\|, \end{aligned}$$

where $\hat{X} := (\hat{x}, \hat{f}_{\hat{x}})$, $\hat{Y} := (\hat{y}, \hat{f}_{\hat{y}})$, and $D \ge 0$ is a constant. Note that we are able to achieve the above

bound because of uniform boundedness of the evaluation functional $\mathcal{E}_{x(t)}$. Thus, for each $t \geq 0$, the map $\hat{X} \mapsto \mathcal{F}(t, \hat{X})$ is uniformly globally Lipschitz continuous. We also note that the map $t \mapsto \mathcal{F}(t, \hat{X})$ is continuous for each $\hat{X} \in \mathbb{X}$ since u is continuous. Using Theorem 1.2 in Chapter 6 of Pazy [75], we can conclude that the above initial value problem has a unique mild solution, and the map $\hat{X}_0 \equiv (\hat{\boldsymbol{x}}_0, \hat{f}_0) \mapsto (\hat{\boldsymbol{x}}, \hat{f})$ is Lipschitz continuous from $\mathbb{X}$ to $C([0, T], \mathbb{X})$. □

Suppose that $\tilde{\boldsymbol{x}}(t) := \boldsymbol{x}(t) - \hat{\boldsymbol{x}}(t)$ and $\tilde{f}(t, \cdot) := f(\cdot) - \hat{f}(t, \cdot)$ denote the state error and the function error, respectively. Equations 11, 12 and 13 can now be expressed in terms of the error equation

$$\begin{Bmatrix} \dot{\tilde{\boldsymbol{x}}}(t) \\ \dot{\tilde{f}}(t) \end{Bmatrix} = \begin{bmatrix} A & B_N \mathcal{E}_{\boldsymbol{x}(t)} \\ -\Gamma^{-1}(B_N \mathcal{E}_{\boldsymbol{x}(t)})^* P & 0 \end{bmatrix} \begin{Bmatrix} \tilde{\boldsymbol{x}}(t) \\ \tilde{f}(t) \end{Bmatrix}. \tag{16}$$

Note, the above equation evolves in $\mathbb{R}^d \times \mathcal{H}_X$. Also, even though the original Eq. 11 and the estimator Eq. 12 are not the same as in Reference [60], the above error equation does have the same form as that studied in Bobade et al. [60]. The existence and uniqueness of a solution for this equation are given by the following theorem.

Theorem 2 *Define $\mathbb{X} := \mathbb{R}^d \times \mathcal{H}_X$, and suppose that $\boldsymbol{x} \in C([0, T]; \mathbb{R}^d)$ and that the embedding $i : \mathcal{H}_X \hookrightarrow C(\Omega)$ is uniform in the sense that there is a constant $C > 0$ such that for any $f \in \mathcal{H}_X$,*

$$\|f\|_{C(\Omega)} \equiv \|if\|_{C(\Omega)} \leq C\|f\|_{\mathcal{H}_X}.$$

Then for any $T > 0$, there is a unique mild solution $(\tilde{\boldsymbol{x}}, \tilde{f}) \in C([0, T], \mathbb{X})$ to Eq. 16 and the map $X_0 \equiv (\tilde{\boldsymbol{x}}_0, \tilde{f}_0) \mapsto (\tilde{\boldsymbol{x}}, \tilde{f})$ is Lipschitz continuous from $\mathbb{X}$ to $C([0, T], \mathbb{X})$.

The proof for this theorem is very similar to the proof of Theorem 1 and is given in Bobade et al. [60]. Note that the above theorem does not study the stability nor the asymptotic stability of the error system. In other words, the convergence of the state error and the function error to the origin is not addressed by this theorem. This aspect is addressed in the following subsection.

3.1 Persistence of excitation

The convergence of state and function errors is guaranteed by additional conditions, commonly referred to as the persistence of excitation (PE) conditions [76–78]. These have been extended to the RKHS framework in Guo et al. [79,80]. This section reviews the persistence of excitation conditions for adaptive estimators on RKHS in detail.

Before taking a look at the PE conditions for the adaptive estimator in the RKHS, it is important to note that they are defined over a set $\Omega \subseteq X$. Now, we can define $\mathcal{H}_\Omega := \overline{\{\mathcal{K}(\boldsymbol{x}, \cdot) | \boldsymbol{x} \in \Omega\}}$. Note that $\mathcal{H}_\Omega$ is a subspace of $\mathcal{H}_X$. The following definitions give us two closely related versions of the PE condition on the set Ω.

Definition 1 (**PE. 1**) The trajectory $\boldsymbol{x} : t \mapsto \boldsymbol{x}(t) \in \mathbb{R}^d$ persistently excites the indexing set Ω and the RKHS $\mathcal{H}_\Omega$ provided there exist positive constants T_0, γ, δ, and Δ, such that for each $t \geq T_0$ and any $g \in \mathcal{H}_X$, there exists $s \in [t, t + \Delta]$ such that

$$\left| \int_s^{s+\delta} \mathcal{E}_{\boldsymbol{x}(\tau)} g \, \mathrm{d}\tau \right| \geq \gamma \|\Pi_\Omega g\|_{\mathcal{H}_X} > 0.$$

Definition 2 (**PE. 2**) The trajectory $\boldsymbol{x} : t \mapsto \boldsymbol{x}(t) \in \mathbb{R}^d$ persistently excites the indexing set Ω and the RKHS $\mathcal{H}_\Omega$ provided there exist positive constants T_0, γ, and Δ such that

$$\int_t^{t+\Delta} \left(\mathcal{E}^*_{\boldsymbol{x}(\tau)} \mathcal{E}_{\boldsymbol{x}(\tau)} g, g \right)_{\mathcal{H}_X} \mathrm{d}\tau \geq \gamma \|\Pi_\Omega g\|^2_{\mathcal{H}_X} > 0$$

for all $t \geq T_0$ and any $g \in \mathcal{H}_X$.

In the above definitions, the term Π_Ω represents the orthogonal projection operator from the RKHS $\mathcal{H}_X$ to its subspace $\mathcal{H}_\Omega$. Notice that both the PE conditions are defined on the set Ω. It would be ideal if $\Omega = X$, the space on which the nonlinear function is defined. However, in most practical applications, the set Ω is a subset of the state space X. The following theorem relates both the PE conditions given above.

Theorem 3 *The PE condition in Definition PE. 1 implies the one in Definition PE. 2. Further, if the family of functions defined by $\{g(\boldsymbol{x}(\cdot)) : t \mapsto g(\boldsymbol{x}(t)) | g \in \mathcal{H}_X\}$ is uniformly equicontinuous, then the PE condition in Definition PE. 2 implies the one in Definition PE. 1,*

With the PE conditions defined, the following theorem addresses the convergence of the states of the error system to the origin.

Theorem 4 *Suppose the trajectory $\boldsymbol{x} : t \mapsto \boldsymbol{x}(t)$ persistently excites the RKHS $\mathcal{H}_\Omega$ in the sense of Definition PE. 1. Then the estimation error system in Eq. 16 is uniformly asymptotically stable at the origin. In particular, we have*

$$\lim_{t\to\infty} \|\tilde{\boldsymbol{x}}(t)\| = 0, \qquad \lim_{t\to\infty} \|\Pi_\Omega \tilde{f}(t)\|_{\mathcal{H}_X} = 0.$$

The proof for this theorem can be found in Guo et al. [79,80]. Intuitively, the second PE condition implies that the state trajectory should repeatedly enter every neighborhood of all the points in the set Ω infinitely many times. To satisfy this, it makes sense to pick the set Ω to be the positive limit set $\omega^+(\boldsymbol{x}_0)$ or one of its subsets. The following theorem from Kurdila et al. [81] affirms that the persistently excited sets are in fact contained in the positive limit set.

Theorem 5 *Let $\mathcal{H}_X$ be the RKHS of functions over X and suppose that this RKHS includes a rich family of bump functions. If the PE condition in Definition PE. 2 holds for Ω, then $\Omega \subseteq \omega^+(\boldsymbol{x}_0)$, the positive limit set corresponding to the initial condition $\boldsymbol{x}_0$.*

3.2 Finite-dimensional approximation

As mentioned above, the evolution of the error equation and the learning law for the RKHS adaptive estimator is in $\mathbb{R} \times \mathcal{H}_X$. In essence, the learning law constitutes a distributed parameter system since $\tilde{f}(t)$ evolves in a infinite-dimensional space. Thus, to implement this adaptive estimator, the persistently excited infinite-dimensional space $\mathcal{H}_\Omega$ is approximated by a nested, dense collection $\{\mathcal{H}_n\}_{n\in\mathbb{N}}$ of finite-dimensional subspaces. Recall that even though the particular nonlinear function f based on the choice of constitutive nonlinearities in Eq. 1 is a function $f = f(x_1)$, we have elected to cast the problem in terms of the more general nonlinear function $f = f(x_1, x_2)$. In this section, we will continue with the analysis of finite-dimensional approximation for the more general unknown nonlinear function $f = f(x_1, x_2)$, which results in Eqs. 17 and 18. Modifications of these equations to study the particular case in which $f = f(x_1)$ are straightforward, and we summarize this specific case at the beginning of Sect. 5. We leave the details to the reader. Let Π_n represent the projection operator from infinite-dimensional $\mathcal{H}_X$ to the finite-dimensional $\mathcal{H}_n$. Now, the finite-dimensional approximations of the adaptive estimator equations can be expressed as

$$\dot{\hat{\boldsymbol{x}}}_n(t) = A\hat{\boldsymbol{x}}_n(t) + B\mathrm{u}(t) + B_N \mathcal{E}_{\boldsymbol{x}(t)} \Pi_n^* \hat{f}_n(t), \tag{17}$$

$$\dot{\hat{f}}_n(t) = \Gamma^{-1} \left(B_N \mathcal{E}_{\boldsymbol{x}(t)} \Pi_n^*\right)^* P \tilde{\boldsymbol{x}}_n(t), \tag{18}$$

where $\tilde{\boldsymbol{x}}_n := \boldsymbol{x} - \hat{\boldsymbol{x}}_n$.

Theorem 6 *Suppose that $\boldsymbol{x} \in C([0, T], \mathbb{R}^d)$ and that the embedding $i : \mathcal{H}_X \hookrightarrow C(\Omega)$ is uniform in the sense that*

$$\|f\|_{C(\Omega)} \equiv \|if\|_{C(\Omega)} \leq C\|f\|_{\mathcal{H}_X}.$$

Then for any $T > 0$,

$$\|\hat{\boldsymbol{x}} - \hat{\boldsymbol{x}}_n\|_{C([0,T];\mathbb{R}^d)} \to 0,$$
$$\|\hat{f} - \hat{f}_n\|_{C([0,T];\mathbb{R}^d)} \to 0,$$

as $n \to \infty$.

The proof of the above theorem can be found in Bobade et al. [60]. As noted earlier, the estimator equations considered in Bobade et al. [60] are different from the ones considered in this paper. However, the error equations for $\hat{\boldsymbol{x}} - \hat{\boldsymbol{x}}_n$ and $\hat{f} - \hat{f}_n$ still have the same form as in Bobade et al. [60], and the proof of the above theorem will remain the same.

4 RKHS adaptive estimator implementation

The previous section discussed the theory behind estimators that evolve in an RKHS. This section presents the algorithm for the implementation of the theory. Figure 2 shows the block diagram of the adaptive estimator. The actual model shown in the figure corresponds to the true system excited by the input , and we assume that we can measure all the states $\boldsymbol{x}(t)$ of this true system. The estimator and learning law blocks in the diagram are what we implement on the computer. Let us first take a look at the estimator model. The operator Π_n^* in the estimator model is the adjoint of the orthogonal projection/approximation operator Π_n. It is equivalent to the inclusion map that maps an element of $\mathcal{H}_n$ space to the same element in the $\mathcal{H}_X$ space. Thus, the term $\mathcal{E}_{x(t)} \Pi_n^* \hat{f}_n(t)$ in the estimator model is the same as $\mathcal{E}_{\boldsymbol{x}(t)} \hat{f}_n(t) = \hat{f}_n(t, \boldsymbol{x}(t))$.

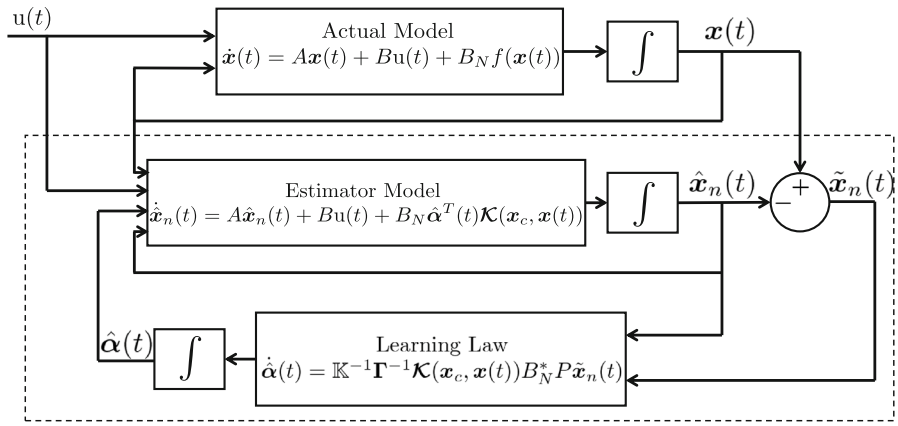

Fig. 2 Adaptive parameter estimator block diagram

Now, let us take a look at the learning law given in Eq. 18. It is a derivative of a function, and we cannot directly implement it on a computer. To convert it to a form that is solvable using numerical methods, we take the inner product of the learning law with $\mathcal{K}(\boldsymbol{x}_i, \cdot)$. Before proceeding with this step, let us recall that the finite-dimensional function estimate $\hat{f}_n(t, \cdot)$ can be expressed as $\hat{f}_n(t, \cdot) = \sum_{j=1}^n \hat{\alpha}_j(t)\mathcal{K}(\boldsymbol{x}_j, \cdot) = \hat{\boldsymbol{\alpha}}^T(t)\mathcal{K}(\boldsymbol{x}_c, \cdot)$. Thus, for $i = 1, \ldots, n$,

$$\left(\mathcal{K}(\boldsymbol{x}_i, \cdot), \dot{\hat{f}}_n(t)\right)_{\mathcal{H}_X} = \left(\mathcal{K}(\boldsymbol{x}_i, \cdot), \Gamma^{-1}\left(B_N\mathcal{E}_{\boldsymbol{x}(t)}\Pi_n^*\right)^* P\tilde{\boldsymbol{x}}_n(t)\right)_{\mathcal{H}_X},$$

which implies

$$\sum_{j=1}^n \mathcal{K}(\boldsymbol{x}_i, \boldsymbol{x}_j)\dot{\hat{\alpha}}_j(t) = \Gamma^{-1}\left(B_N\mathcal{E}_{\boldsymbol{x}(t)}\mathcal{K}(\boldsymbol{x}_i, \cdot), P\tilde{\boldsymbol{x}}_n(t)\right)_{\mathcal{H}_X}.$$

Thus, if $\hat{\boldsymbol{\alpha}}(t) := \{\hat{\alpha}_1(t), \ldots, \hat{\alpha}_n(t)\}^T$, its time derivative is given by the expression

$$\dot{\hat{\boldsymbol{\alpha}}}(t) = \mathbb{K}^{-1}\boldsymbol{\Gamma}^{-1}\mathcal{K}(\boldsymbol{x}_c, \boldsymbol{x}(t))B_N^* P\tilde{\boldsymbol{x}}_n(t),$$

where $\mathbb{K}$ is the symmetric positive definite Grammian matrix whose ij^{th} element is defined as $\mathbb{K}_{ij} := \mathcal{K}(\boldsymbol{x}_i, \boldsymbol{x}_j)$, $\boldsymbol{\Gamma} := \Gamma\mathbb{I}_n$ is the gain matrix, and

$$\mathcal{K}(\boldsymbol{x}_c, \boldsymbol{x}(t)) := \left\{\mathcal{K}(\boldsymbol{x}_1, \boldsymbol{x}(t)), \ldots, \mathcal{K}(\boldsymbol{x}_n, \boldsymbol{x}(t))\right\}^T.$$

The above equation gives us an expression for the rate at which the coefficients of the kernels change with time. Therefore, the implementation of the adaptive estimator amounts to integration of the equations

$$\dot{\hat{\boldsymbol{x}}}_n(t) = A\hat{\boldsymbol{x}}_n(t) + B\mathrm{u}(t) + B_N\hat{\boldsymbol{\alpha}}^T(t)\mathcal{K}(\boldsymbol{x}_c, \boldsymbol{x}(t)), \tag{19}$$

$$\dot{\hat{\boldsymbol{\alpha}}}(t) = \mathbb{K}^{-1}\boldsymbol{\Gamma}^{-1}\mathcal{K}(\boldsymbol{x}_c, \boldsymbol{x}(t))B_N^* P\tilde{\boldsymbol{x}}_n(t). \tag{20}$$

From the discussion in Sect. 3.1, it is clear that the persistence of excitation is sufficient to ensure parameter convergence. However, it is hard and sometimes impossible to check if a given space is persistently exciting. The following theorem from Kurdila et al. [82] gives us a sufficient condition for the persistence of excitation that is easy to verify. However, this theorem is only applicable to cases where radial basis functions over $\mathbb{R}^d$ generate the RKHS. Furthermore, we can only use this sufficient condition to check the persistence of excitation of finite-dimensional spaces. However, since all implementation is in the finite-dimensional spaces, the following theorem provides us a powerful tool to verify the convergence of parameters in practical applications.

Theorem 7 *Let* $\epsilon < \frac{1}{2}\min_{i\neq j}\|\boldsymbol{x}_i - \boldsymbol{x}_j\|$, *where* $\boldsymbol{x}_i$ *and* $\boldsymbol{x}_j$ *are the kernel centers* $\{\boldsymbol{x}_1, \ldots, \boldsymbol{x}_n\}$. *For every* $t_0 \geq 0$ *and* $\delta > 0$, *define*

$$I_i = \{t \in [t_0, t_0 + \delta] : \|\boldsymbol{x}(t) - \boldsymbol{x}_i\| \leq \epsilon\}.$$

If there exists a δ *such that the measure of* I_i *is bounded below by a positive constant that is independent of* t_0 *and the kernel center* $\boldsymbol{x}_i$, *and if the measure of* $[t_0, t_0+\delta]$ *less than or equal to* δ, *then the space* $\mathcal{H}_n$ *is persistently exciting in the sense of Definition PE. 2.*

We have to note that the persistence of excitation of $\mathcal{H}_n$ does not imply the convergence of error to 0 since the function f belongs to the infinite-dimensional space $\mathcal{H}_X$. However, it can be shown that $\text{limsub}_{t\to\infty} \left\| \Pi_n \left(f - \hat{f}_n(t) \right) \right\|_{\mathcal{H}_X}$ is bounded above by a positive constant when, for any t, the function $\left(f - \hat{f}_n(t) \right)$ belongs to a family of uniformly equicontinuous functions and x is uniformly continuous. We refer the reader to Kurdilaet al: [82] for a more detailed discussion on the convergence of parameters in finite-dimensional spaces.

The following algorithm gives a step-by-step procedure for implementing the RKHS adaptive estimator.

Algorithm 1: RKHS adaptive estimator implementation

Input: $\boldsymbol{x}(t)$,$w^+(\boldsymbol{x}_0)$
Output: $\hat{f}_n(T, \cdot)$

1 Choose the RKHS $\mathcal{H}_X$ and the corresponding reproducing kernel $\mathcal{K}(\cdot, \cdot)$.
2 Choose kernel centers $\boldsymbol{x}_i$, for $i = 1, \ldots, N$ uniformly distributed on $w^+(\boldsymbol{x}_0)$,
if X is equal to the state space, choose kernels centers on $w^+(\boldsymbol{x}_0)$,
if X is a proper subset of the state space, choose kernel centers on the projection of $w^+(\boldsymbol{x}_0)$ on to the space X.
3 Run the adaptive estimator until the parameters converge. Integrate

$$\dot{\hat{\boldsymbol{x}}}_n(t) = A\hat{\boldsymbol{x}}_n(t) + B\mathrm{u}(t) + B_N\hat{\boldsymbol{\alpha}}^T(t)\boldsymbol{\mathcal{K}}(\boldsymbol{x}_c, \boldsymbol{x}(t)),$$
$$\dot{\hat{\boldsymbol{\alpha}}}(t) = \mathbb{K}^{-1}\boldsymbol{\Gamma}^{-1}\boldsymbol{\mathcal{K}}(\boldsymbol{x}_c, \boldsymbol{x}(t))B_N^* P\tilde{\boldsymbol{x}}_n(t)$$

over the interval $[0, T]$.
4 Define $\hat{f}_n(T, \cdot) := \hat{\boldsymbol{\alpha}}^T(T)\boldsymbol{\mathcal{K}}(\boldsymbol{x}_c, \cdot)$.

5 Numerical simulation results

In this section, we consider the prototypical piezoelectric oscillator example modeled in Sect. 2 to study the effectiveness of an RKHS adaptive estimator and make qualitative studies of convergence. As emphasized above, the finite-dimensional Eqs. 17 and 18 are stated for the general analysis when the unknown function $f = f(x_1, x_2)$. In this section, we study qualitative convergence properties in the specific case that $f = f(x_1)$. For this specific example, it is straightforward to show that the finite-dimensional equations have the form

$$\dot{\hat{\boldsymbol{x}}}_n(t) = A\hat{\boldsymbol{x}}_n(t) + B\mathrm{u}(t) + B_N\mathcal{E}_{x_1(t)}\Pi_n^*\hat{f}_n(t),$$
$$\dot{\hat{f}}_n(t) = \Gamma^{-1}\left(B_N\mathcal{E}_{x_1(t)}\Pi_n^*\right)^* P\tilde{\boldsymbol{x}}_n(t).$$

These equations evolve in $\mathbb{R}^d \times \mathcal{H}_n$, where

$$\mathcal{H}_n = span\{\mathcal{K}(x_{1,i}, \cdot)\}$$

is defined in terms of the kernel on $\mathbb{R}$, $\mathcal{K} : \mathbb{R} \times \mathbb{R} \to \mathbb{R}$ and displacement samples $\boldsymbol{x}_c = \{x_{1,i}\}_{i=1}^n = \Omega_n \subseteq \Omega \subseteq \mathbb{R}$. With this interpretation and the definition $\mathcal{K}(\boldsymbol{x}_c, \boldsymbol{x}(t)) := \{\mathcal{K}(x_{1,1}, x_1(t)), \ldots, \mathcal{K}(x_{1,n}, x_1(t))\}^T$, the specific governing equations still have the form shown in Eqs. 19, 20, and Algorithm 4 applies. Tables 1 and 2 list the numerical values of the parameters used to build the actual model shown in Eq. 10. We used the shape function corresponding to the first cantilever beam mode while modeling the system to get Eqs. 8 and 9 . Table 2 also shows the input used to drive the actual system.

Figure 3 shows the steady-state response of the actual piezoelectric system. This figure gives us an estimate of maximum and minimum displacement. Under the assumption that the unknown nonlinear term is a function of displacement only, it is clear that the set $\Omega \subseteq \mathbb{R}$. For this problem, the set Ω is the closed interval from minimum displacement to the maximum displacement. For the adaptive estimator, the reproducing kernel implemented in the simulation was selected to be the popular exponential function

Table 1 Piezoceramic parameters used in simulations

	Parameter	Value
Piezoceramic (PIC 151)	ρ_p	7790 (kg/m^3)
	h_p	0.001 (m)
	a	0
	b	l
	$d_{31,0}$	−2.1e−10 (m/V)
	$d_{31,1}$	−36.9746 (m/V)
	$d_{31,2}$	−0.03596 (m/V)
	E_{p0}	0.667e+11 (Pa)
	E_{p1}	−3.328e−12 (Pa)
	E_{p2}	−1.4e+18 (Pa)
	ϵ_{33}	2.12e−8 (F/m)

Table 2 Other parameters of the actual system used in simulations

	Parameter	Value
Substrate	Material	St 37
	ρ_b	7800 (kg/m^3)
	C_b	2.089e+11 (Pa)
	l	0.4 (m)
	b	0.025 (m)
	h	0.003 (m)
Damping	α	0.1
	β	1e-3
Input	u(t)	$A\sin(\omega t)$
	Amplitude A	1 (m/s^2)
	Frequency ω	22.5 (rad/s)

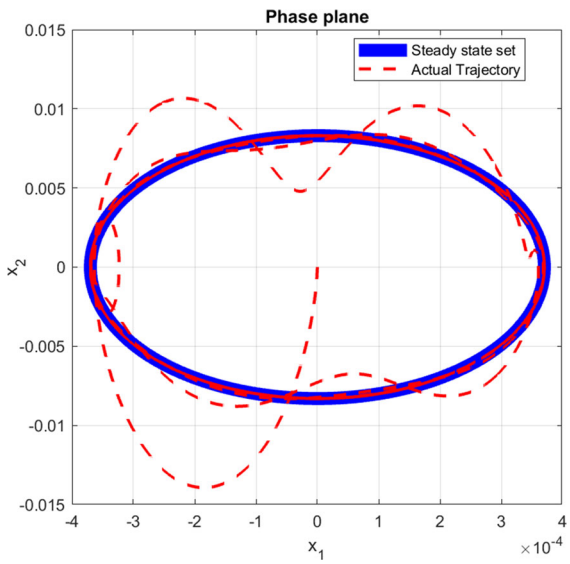

Fig. 3 The trajectory in the phase plane starting at $[0, 0]^T$ eventually converges to the steady-state set

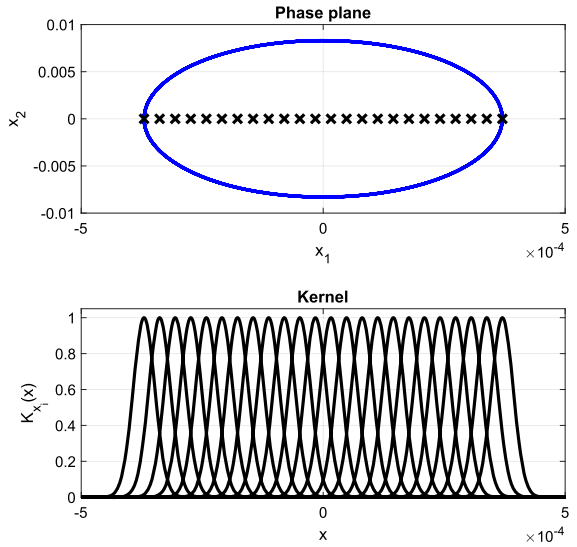

Fig. 4 Radial basis functions centered at equidistant points in Ω

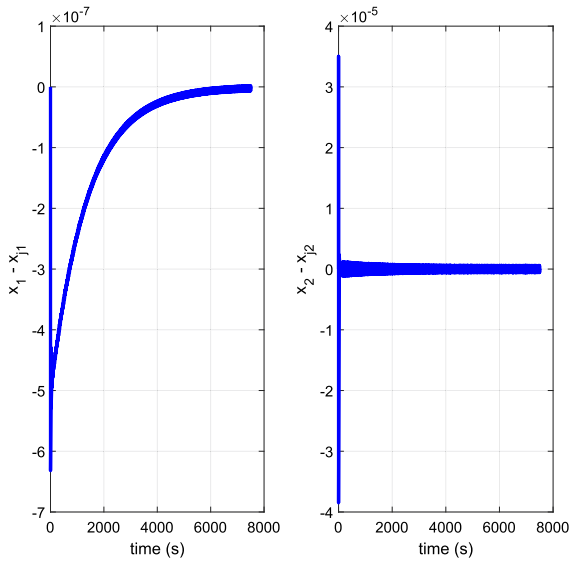

Fig. 5 Evolution of state error with time

$$\mathcal{K}(x, y) = e^{-\frac{||x-y||^2}{2\sigma^2}}.$$

Thus, $\mathcal{H}_\Omega$ is the set defined as

$$\mathcal{H}_\Omega := \overline{\{\mathcal{K}(x, \cdot) = e^{-\frac{||x-\cdot||^2}{2\sigma^2}} | x \in \Omega \subseteq \mathbb{R}\}},$$

where σ is the standard deviation of the radial basis function. For the simulations, we used $\sigma = 1e-9$. As shown in Fig. 4, a total of 24 equidistant points were chosen in the interval $\Omega = [-0.00037018, 0.00037026]$ and the kernel functions were centered at these points. It is clear from the state-state trajectory in Fig. 3 that the hypotheses for the sufficient condition given in Theorem 7 are satisfied.

Figure 5 shows the time history of the state errors. As expected, the state errors eventually converge to zero. Figure 6 shows the final 500-time-steps of the

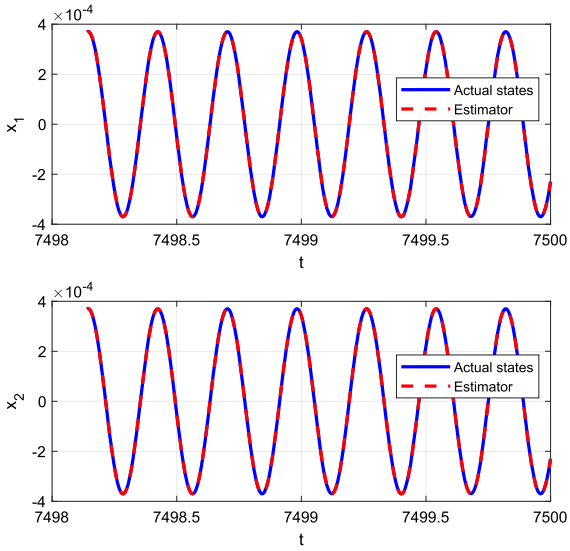

Fig. 6 Actual states and state estimate—final 500 timesteps

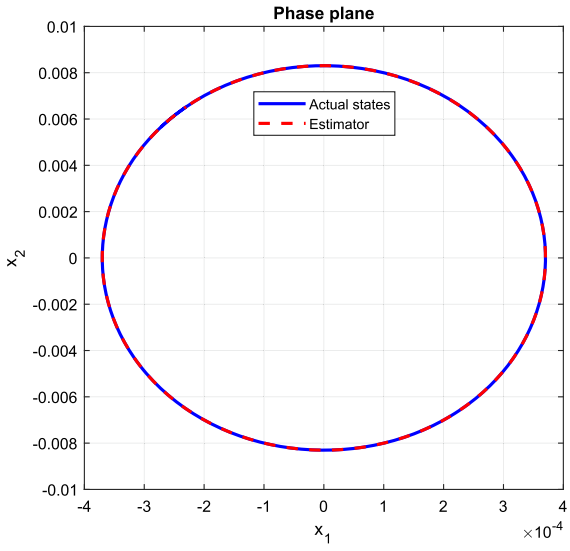

Fig. 7 Actual states and state estimates in phase plane after convergence of state error

actual states and the estimated states. Figure 7 shows the corresponding phase plot. It is clear from these plots that the estimator tracks the actual states with almost no error.

Figures 8, 9, 10 and 11 show the evolution of the parameters. It is clear from the figures that the estimated parameters converge to a constant as time $t \to \infty$.

The plot of the actual function f and estimated function $\hat{f}_i$ evaluated on $\mathbb{R}$ can be seen in Fig. 12. Figure 13

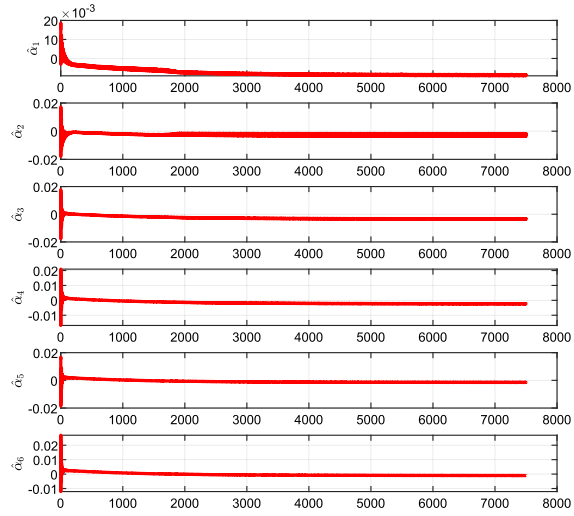

Fig. 8 Evolution of the parameter estimates $\hat{\alpha}_1 - \hat{\alpha}_6$ with time

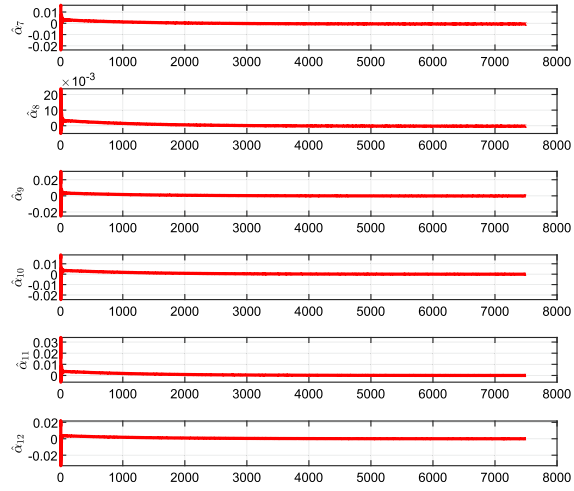

Fig. 9 Evolution of the parameter estimates $\hat{\alpha}_7 - \hat{\alpha}_{12}$ with time

shows the pointwise error between the actual and estimated functions. The figures show that the actual and estimated functions agree on Ω. Recall that convergence of the function error is guaranteed on the set Ω in the norm on $\mathcal{H}_X$ essentially. This amounts to a guarantee of the pointwise error over the set Ω. No guarantee is made for values outside Ω. See [79–81] for more details on the convergence.

6 Conclusion

This paper has introduced a novel approach to model and estimate uncertain nonlinear piezoelectric oscilla-

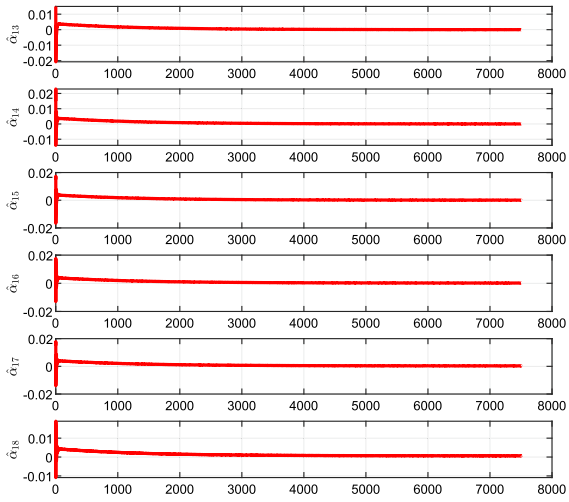

Fig. 10 Evolution of the parameter estimates $\hat{\alpha}_{13} - \hat{\alpha}_{18}$ with time

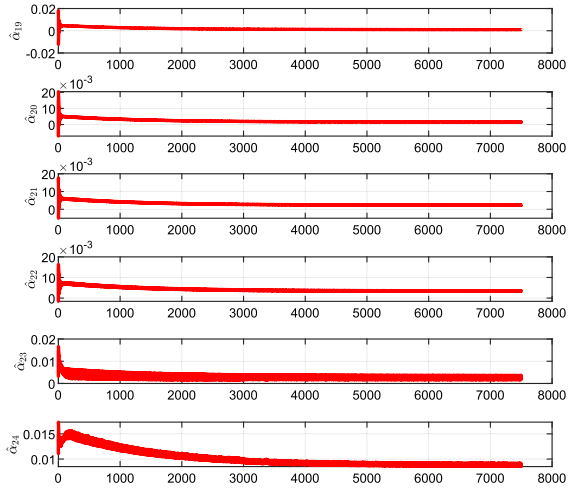

Fig. 11 Evolution of the parameter estimates $\hat{\alpha}_{19} - \hat{\alpha}_{24}$ with time

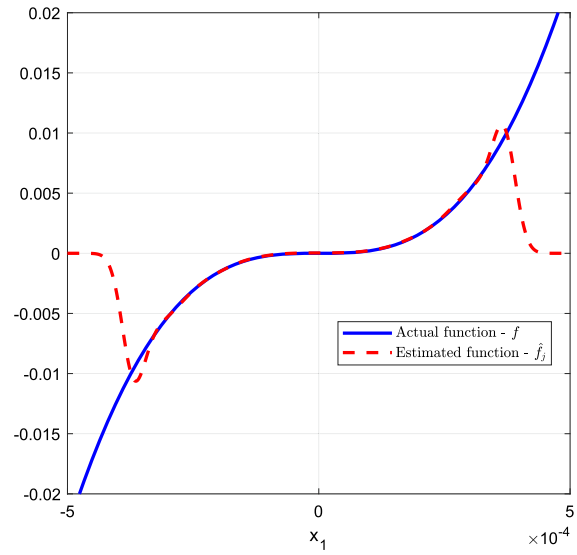

Fig. 12 Actual function and function estimate on $\mathbb{R}$

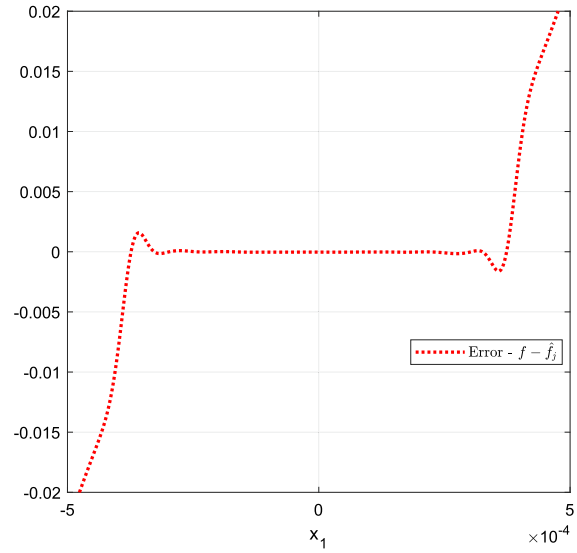

Fig. 13 Error between actual function and function estimate on $\mathbb{R}$

tors, and the effectiveness of the approach has been validated by testing it on a nonlinear piezoelectric bimorph beam. The nonlinear function used in the numerical study depended only on the displacement, but much of the theory applies to more complex uncertainties. It would be of interest to study the effectiveness of such estimators on more complex oscillators, ones for which unknown nonlinearities depend on all the states. The algorithm discussed in this paper follows a general framework and can be adapted easily to model many other nonlinearities. Robustness of the current algorithm and its effectiveness in the presence of noise would be of great interest and remains to be explored and would complement the findings in the current study.

Compliance with ethical standards

Conflict of interest The authors declare that they have no conflict of interest.

A Piezoelectric oscillator—governing equations

In this section, we go over the detailed steps involved in the derivation of the infinite-dimensional governing equation of the piezoelectric oscillator as shown in Fig. 1. The kinetic energy and the electric potential are given by Eqs. 3 and 5, respectively. Using Hamilton's principle, we get the variational identity

$$\begin{aligned}
&\delta\int_{t_0}^{t_1}(T-\mathcal{V}_{\mathcal{H}})\mathrm{d}t\\
&=\delta\int_{t_0}^{t_1}\left\{\left[\frac{1}{2}\mathrm{m}\int_0^l(\dot{w}+\dot{z})^2\mathrm{d}x\right]\right.\\
&\quad-\left[\frac{1}{2}C_bI_b\int_0^l(w'')^2\mathrm{d}x+2a_{(0,2)}\int_a^b(w'')^2\mathrm{d}x\right.\\
&\quad+2a_{(2,4)}\int_a^b(w'')^4\mathrm{d}x+2b_{(1,1)}\left[\int_a^b w''\mathrm{d}x\right]E_z\\
&\quad\left.\left.+2b_{(3,1)}\left[\int_a^b(w'')^3\mathrm{d}x\right]E_z-2b_{(0,2)}E_z^2\right]\right\}\mathrm{d}t=0.
\end{aligned}\tag{21}$$

The above variational statement can be rewritten as

$$\begin{aligned}
\delta\int_{t_0}^{t_1}(T-\mathcal{V}_{\mathcal{H}})\mathrm{d}t&=\int_{t_0}^{t_1}\left\{\int_0^l\mathrm{m}\dot{w}\delta\dot{w}+\mathrm{m}\dot{z}\delta\dot{w})\mathrm{d}x\right.\\
&-\int_0^l C_bI_bw''\delta w''\mathrm{d}x-4a_{(0,2)}\int_a^b w''\delta w''\mathrm{d}x\\
&-8a_{(2,4)}\int_a^b(w'')^3\delta w''\mathrm{d}x-2b_{(1,1)}\left(\int_a^b(\delta w'')\mathrm{d}x\right)E_z\\
&-2b_{(1,1)}\left(\int_a^b w''\mathrm{d}x\right)\delta E_z\\
&-6b_{(3,1)}\left(\int_a^b(w'')^2\delta w''\mathrm{d}x\right)E_z\\
&-2b_{(3,1)}\left(\int_a^b(w'')^3\mathrm{d}x\right)\delta E_z\\
&\left.+4b_{(0,2)}E_z\delta E_z\right\}\mathrm{d}t=0
\end{aligned}\tag{22}$$

After integrating the above statement by parts, we get

$$\begin{aligned}
&\int_{t_0}^{t_1}\left\{-\int_0^l\left[\mathrm{m}\ddot{w}+\mathrm{m}\ddot{z}+C_bI_bw''''\right.\right.\\
&+4a_{(0,2)}\left(\chi_{[a,b]}w''\right)''+8a_{(2,4)}(\chi_{[a,b]}(w'')^3)''\\
&\left.+2b_{(1,1)}\chi''_{[a,b]}E_z+6b_{(3,1)}(\chi_{[a,b]}(w'')^2)''E_z\right]\delta w\mathrm{d}x\\
&-\left[2b_{(1,1)}\left(\int_0^l\chi_{[a,b]}w''\mathrm{d}x\right)\right.\\
&\left.+2b_{(3,1)}\left(\int_0^l\chi_{[a,b]}(w'')^3\mathrm{d}x\right)-4b_{(0,2)}E_z\right]\delta E_z\\
&-\left\{C_bI_bw''+4a_{(0,2)}\chi_{[a,b]}w''+8a_{(2,4)}\chi_{[a,b]}(w'')^3\right.\\
&\left.+2b_{(1,1)}\chi_{[a,b]}E_z+6b_{(3,1)}\chi_{[a,b]}(w'')^2\right\}\delta w'\Big|_0^l\\
&+\left\{C_bI_bw'''+4a_{(0,2)}\left(\chi_{[a,b]}w''\right)'\right.\\
&+8a_{(2,4)}\left(\chi_{[a,b]}(w'')^3\right)'\\
&+2b_{(1,1)}\chi'_{[a,b]}E_z+6b_{(3,1)}\\
&\left.\left.\left(\chi_{[a,b]}(w'')^2\right)'\right\}\delta w\Big|_0^l\right\}\mathrm{d}t=0.
\end{aligned}$$

Note, in the above statement, the term $\chi_{[a,b]}$ is called the characteristic function of $[a,b]$ and is defined as

$$\chi_{[a,b]}(x):=\begin{cases}1 \text{ if } x\in[a,b],\\ 0 \text{ if } x\notin[a,b].\end{cases}\tag{23}$$

Since the variation of w and E_z are arbitrary, we can conclude that the equations of motion of the nonlinear piezoelectric cantilevered bimorph have the form shown in Eqs. 6 and 7.

B Single mode approximation of the piezoelectric oscillator equations

As mentioned earlier, the effects of nonlinearity in piezoelectric oscillators are most noticeable near the natural frequency of the system. Hence, single-mode models are sufficient to model the dynamics as long as the range of input excitation is restricted to a band around the first natural frequency. Let us introduce the single-mode approximation $w(x,t)=\psi(x)u(t)$. To make calculations easier, let us introduce this approximation into the variational statement shown in Eq. 22. Further, note that

$$\begin{aligned}
\int_{t_0}^{t_1}\int_0^l\mathrm{m}\dot{w}\delta\dot{w}\mathrm{d}x\mathrm{d}t&=-\int_{t_0}^{t_1}\int_0^l\mathrm{m}\ddot{w}\delta w\mathrm{d}x\mathrm{d}t,\\
\int_{t_0}^{t_1}\int_0^l\mathrm{m}\dot{z}\delta\dot{w}\mathrm{d}x\mathrm{d}t&=-\int_{t_0}^{t_1}\int_0^l\mathrm{m}\ddot{z}\delta w\mathrm{d}x\mathrm{d}t.
\end{aligned}$$

After introducing the approximation for $w(x,t)$ into the variational statement in Eq. 22 and using the equations shown above, we get the variational statement

$$
\begin{aligned}
0 = \int_{t_0}^{t_1} \Bigg\{ & -\Bigg[\mathrm{m} \left(\int_0^l \psi^2(x)\mathrm{d}x \right) \ddot{u} + \mathrm{m} \left(\int_0^l \psi(x)\mathrm{d}x \right) \ddot{z} \\
& + C_b I_b \left(\int_0^l \left(\psi''(x)\right)^2 \mathrm{d}x \right) u \\
& + 4a_{(0,2)} \left(\int_0^l \chi_{[a,b]} \left(\psi''(x)\right)^2 \right) u \\
& + 8a_{(2,4)} \left(\int_0^l \chi_{[a,b]} \left(\psi''(x)\right)^4 \mathrm{d}x \right) u^3 \\
& + 2b_{(1,1)} E_z \left(\int_0^l \chi_{[a,b]} \psi''(x)\mathrm{d}x \right) \\
& + 6b_{(3,1)} \left(\int_0^l \chi_{[a,b]} \left(\psi''(x)\right)^3 \right) u^2 E_z \Bigg] \delta u \\
& - \Bigg[2b_{(1,1)} \left(\int_0^l \chi_{[a,b]} \psi''(x)\mathrm{d}x \right) u \\
& + 2b_{(3,1)} \left(\int_0^l \chi_{[a,b]} \left(\psi''(x)\right)^3 \right) u^3 \\
& - 4b_{(0,2)} E_z \Bigg] \delta E_z \Bigg\} \mathrm{d}t
\end{aligned}
$$

Thus, the approximated equation of motion are

$$
\begin{aligned}
& \underbrace{\mathrm{m} \left(\int_0^l \psi^2(x)\mathrm{d}x \right)}_{M} \ddot{u} + \underbrace{\mathrm{m} \left(\int_0^l \psi(x)\mathrm{d}x \right)}_{P} \ddot{z} \\
& + \underbrace{C_b I_b \left(\int_0^l \left(\psi''(x)\right)^2 \mathrm{d}x \right)}_{K_b} u \\
& + \underbrace{4a_{(0,2)} \left(\int_0^l \chi_{[a,b]} \left(\psi''(x)\right)^2 \right)}_{K_p} u \\
& + \underbrace{8a_{(2,4)} \left(\int_0^l \chi_{[a,b]} \left(\psi''(x)\right)^4 \mathrm{d}x \right)}_{K_N} u^3 \\
& + \underbrace{2b_{(1,1)} \left(\int_0^l \chi_{[a,b]} \psi''(x)\mathrm{d}x \right)}_{\mathcal{B}} E_z \\
& + \underbrace{6b_{(3,1)} \left(\int_0^l \chi_{[a,b]} \left(\psi''(x)\right)^3 \right)}_{Q_N} u^2 E_z = 0,
\end{aligned}
$$

$$
\begin{aligned}
& \underbrace{2b_{(1,1)} \left(\int_0^l \chi_{[a,b]} \psi''(x)\mathrm{d}x \right)}_{\mathcal{B}} u(t) \\
& + \underbrace{2b_{(3,1)} \left(\int_0^l \chi_{[a,b]} \left(\psi''(x)\right)^3 \right)}_{\mathcal{B}_N} u^3(t) = \underbrace{4b_{(0,2)}}_{\mathcal{C}} E_z.
\end{aligned}
$$

These calculations generate the approximated Eqs. 8 and 9.

References

1. Banks, H.T., Smith, R.C., Wang, Y.: Smart Material Structures: Modeling, Estimation, and Control. Wiley, New York (1996)
2. Smith, R.C.: Smart Material Systems: Model Development. SIAM, Philadelphia (2005)
3. Leo, D.J.L.: Engineering Analysis of Smart Material Systems. Wiley, New York. https://doi.org/10.1002/9780470209721. arXiv:1107.1180 (2007)
4. Preumont, A.: Mechatronics: Dynamics of Electromechanical and Piezoelectric Systems. Springer, Dordrecht (2006). https://doi.org/10.1007/1-4020-4696-0
5. Erturk, A., Inman, D.J.: Piezoelectric Energy Harvesting. Wiley, Chichester (2011). https://doi.org/10.1002/9781119991151
6. Priya, S., Inman, D.J.: Energy Harvesting Technologies. https://doi.org/10.1007/978-0-387-76464-1. arXiv:1011.1669v3 (2009)
7. Maugin, G.A.: Nonlinear Electromechanical Effects and Applications, vol. 1. World Scientific Publishing Company, New York (1986)
8. Yang, J.: Analysis of Piezoelectric Devices. World Scientific, New York (2006)
9. Yang, J.: An introduction to the theory of piezoelectricity. In: Advances in Mechanics and Mathematics, vol. 9. Springer, Boston. https://doi-org.ezproxy.lib.vt.edu/10.1007/b101799 (2005)
10. Yu, Y.Y.: Vibrations of Elastic Plates: Linear and Nonlinear Dynamical Modeling of Sandwiches, Laminated Composites, and Piezoelectric Layers. Springer, Berlin (2012)
11. von Wagner, U., Hagedorn, P.: Piezo-beam systems subjected to weak electric field: experiments and modelling of non-linearities. J. Sound Vib. **256**(5), 861–872 (2002). https://doi.org/10.1006/jsvi.2002.5024
12. von Wagner, U., Hagedorn, P.: Nonlinear effects of piezoceramics excited by weak electric fields. Nonlinear Dyn. **31**(2), 133–149 (2003). https://doi.org/10.1023/A:1022093428599
13. von Wagner, U.: Non-linear longitudinal vibrations of piezoceramics excited by weak electric fields. Int. J. Non-Linear Mech. **38**(4), 565–574 (2003). https://doi.org/10.1016/S0020-7462(01)00113-5
14. von Wagner, U.: Non-linear longitudinal vibrations of non-slender piezoceramic rods. Int. J. Non-Linear

Mech. **39**(4), 673–688 (2004). https://doi.org/10.1016/S0020-7462(03)00108-2
15. Stanton, S.C., Erturk, A., Mann, B.P., Inman, D.J.: Nonlinear piezoelectricity in electroelastic energy harvesters: modeling and experimental identification. J. Appl. Phys. **108**(7), 74903 (2010). https://doi.org/10.1063/1.3486519
16. Stanton, S.C., Erturk, A., Mann, B.P., Dowell, E.H., Inman, D.J.: Nonlinear nonconservative behavior and modeling of piezoelectric energy harvesters including proof mass effects. J. Intell. Mater. Syst. Struct. **23**(2), 183–199 (2012). https://doi.org/10.1177/1045389X11432656
17. Wolf, K., Gottlieb, O.: Nonlinear dynamics of a noncontacting atomic force microscope cantilever actuated by a piezoelectric layer. J. Appl. Phys. **91**(7), 4701–4709 (2002). https://doi.org/10.1063/1.1458056
18. Usher, T., Sim, A.: Nonlinear dynamics of piezoelectric high displacement actuators in cantilever mode. J. Appl. Phys. **98**(6), 64102 (2005). https://doi.org/10.1063/1.2041844
19. Triplett, A., Quinn, D.D.: The effect of non-linear piezoelectric coupling on vibration-based energy harvesting. J. Intell. Mater. Syst. Struct. **20**(16), 1959–1967 (2009). https://doi.org/10.1177/1045389X09343218
20. Guckenheimer, J., Holmes, P.: Nonlinear Oscillations, Dynamical Systems, and Bifurcations of Vector Fields, vol. 42. Springer, Berlin (2013)
21. Wiggins, S.: Introduction to Applied Nonlinear Dynamical Systems and Chaos, vol. 2. Springer, Berlin (2003)
22. Nayfeh, A.H.: Introduction to Perturbation Techniques. Wiley, Hoboken (2011)
23. Visintin, A.: Differential Models of Hysteresis, vol. 111. Springer, Berlin (2013)
24. Brokate, M., Sprekels, J.: Hysteresis and Phase Transitions, vol. 121. Springer, Berlin (2012)
25. Ge, P., Jouaneh, M.: Modeling hysteresis in piezoceramic actuators. Precis. Eng. **17**(3), 211–221 (1995). https://doi.org/10.1016/0141-6359(95)00002-U
26. Hu, H., Ben Mrad, R.: On the classical Preisach model for hysteresis in piezoceramic actuators. Mechatronics **13**(2), 85–94 (2003). https://doi.org/10.1016/S0957-4158(01)00043-5
27. Xiao, S., Li, Y.: Modeling and high dynamic compensating the rate-dependent hysteresis of piezoelectric actuators via a novel modified inverse Preisach model. IEEE Trans. Control Syst. Technol. **21**(5), 1549–1557 (2013). https://doi.org/10.1109/TCST.2012.2206029
28. Rakotondrabe, M.: Classical Prandtl–Ishlinskii modeling and inverse multiplicative structure to compensate hysteresis in piezoactuators. In: 2012 American Control Conference (ACC), pp. 1646–1651. https://doi.org/10.1109/ACC.2012.6314620 (2012)
29. Qin, Y., Tian, Y., Zhang, D., Shirinzadeh, B., Fatikow, S.: A novel direct inverse modeling approach for hysteresis compensation of piezoelectric actuator in feedforward applications. IEEE/ASME Trans. Mechatron. **18**(3), 981–989 (2013). https://doi.org/10.1109/TMECH.2012.2194301
30. Ang, W.T., Garmon, F.A., Khosla, P.K., Riviere, C.N.: Modeling rate-dependent hysteresis in piezoelectric actuators. In: Proceedings 2003 IEEE/RSJ International Conference on Intelligent Robots and Systems (IROS 2003) (Cat. No.03CH37453), vol. 2, pp. 1975–1980. https://doi.org/10.1109/IROS.2003.1248937 (2003)
31. Zhang, Y.L., Han, M.L., Yu, M.Y., Shee, C.Y., Ang, W.T.: Automatic hysteresis modeling of piezoelectric micromanipulator in vision-guided micromanipulation systems. IEEE/ASME Trans. Mechatron. **17**(3), 547–553 (2012). https://doi.org/10.1109/TMECH.2011.2106136
32. Li, Z., Shan, J., Gabbert, U.: Inverse compensation of hysteresis using Krasnoselskii–Pokrovskii model. IEEE/ASME Trans. Mechatron. **23**(2), 966–971 (2018). https://doi.org/10.1109/TMECH.2018.2805761
33. Banks, H.T., Kurdila, A.J., Webb, G.: Identification of hysteretic control influence operators representing smart actuators part I: formulation. Math. Prob. Eng. **3**, 723495 (1997). https://doi.org/10.1155/S1024123X97000586
34. Galinaitis, W.S., Rogers, R.C.: Control of a hysteretic actuator using inverse hysteresis compensation. In: Proc. SPIE, vol. 3323. https://doi.org/10.1117/12.316308 (1998)
35. Goldfarb, M., Celanovic, N.: Modeling piezoelectric stack actuators for control of micromanipulation. IEEE Control Syst. Mag. **17**(3), 69–79 (1997). https://doi.org/10.1109/37.588158
36. Liu, Y., Shan, J., Gabbert, U., Qi, N.: Hysteresis and creep modeling and compensation for a piezoelectric actuator using a fractional-order Maxwell resistive capacitor approach. Smart Mater. Struct. **22**(11), 115020 (2013). https://doi.org/10.1088/0964-1726/22/11/115020
37. Zhu, W., Rui, X.T.: Hysteresis modeling and displacement control of piezoelectric actuators with the frequency-dependent behavior using a generalized Bouc–Wen model. Precis. Eng. **43**, 299–307 (2016). https://doi.org/10.1016/j.precisioneng.2015.08.010
38. Rakotondrabe, M.: Bouc–Wen modeling and inverse multiplicative structure to compensate hysteresis nonlinearity in piezoelectric actuators. IEEE Trans. Autom. Sci. Eng. **8**(2), 428–431 (2011). https://doi.org/10.1109/TASE.2010.2081979
39. Low, T.S., Guo, W.: Modeling of a three-layer piezoelectric bimorph beam with hysteresis. J. Microelectromech. Syst. **4**(4), 230–237 (1995). https://doi.org/10.1109/84.475550
40. Xu, Q., Li, Y.: Dahl model-based hysteresis compensation and precise positioning control of an XY parallel micromanipulator with piezoelectric actuation. J. Dyn. Syst., Meas., Control (2010). https://doi.org/10.1115/1.4001712
41. Shome, S.K., Prakash, M., Mukherjee, A., Datta, U.: Dither control for Dahl model based hysteresis compensation. In: 2013 IEEE International Conference on Signal Processing, Computing and Control (ISPCC), pp. 1–6. https://doi.org/10.1109/ISPCC.2013.6663460 (2013)
42. Lin, C.J., Lin, P.T.: Tracking control of a biaxial piezo-actuated positioning stage using generalized Duhem model. Comput. Math. Appl. **64**(5), 766–787 (2012). https://doi.org/10.1016/j.camwa.2011.12.015
43. Xie, W., Fu, J., Yao, H., Su, C.: Observer based control of piezoelectric actuators with classical Duhem modeled hysteresis. In: 2009 American Control Conference, pp. 4221–4226. https://doi.org/10.1109/ACC.2009.5159851 (2009)
44. Gan, J., Zhang, X.: A review of nonlinear hysteresis modeling and control of piezoelectric actuators. AIP Adv. **9**(4), 40702 (2019). https://doi.org/10.1063/1.5093000
45. Ewins, D.J.: Modal Testing: Theory and Practice, vol. 15. Research Studies Press Letchworth (1984)

46. Kao, C.C., Fung, R.F.: Using the modified PSO method to identify a Scott–Russell mechanism actuated by a piezoelectric element. Mech. Syst. Sig. Process. **23**(5), 1652–1661 (2009). https://doi.org/10.1016/j.ymssp.2008.12.003
47. Fung, R.F., Hsu, Y.L., Huang, M.S.: System identification of a dual-stage XY precision positioning table. Precis. Eng. **33**(1), 71–80 (2009). https://doi.org/10.1016/j.precisioneng.2008.04.002
48. Chen, C.M., Hsu, Y.C., Fung, R.F.: System identification of a Scott–Russell amplifying mechanism with offset driven by a piezoelectric actuator. Appl. Math. Modell. **36**(6), 2788–2802 (2012). https://doi.org/10.1016/j.apm.2011.09.064
49. Kutz, J., Brunton, S., Brunton, B., Proctor, J.: Dynamic mode decomposition: data-driven modeling of complex systems. Soc. Ind. Appl. Math. **10**(1137/1), 9781611974508 (2016)
50. Tu, J.H., Rowley, C.W., Luchtenburg, D.M., Brunton, S.L., Kutz, J.N.: On dynamic mode decomposition: theory and applications. J. Comput. Dyn. **1**(2), 391–421 (2014). https://doi.org/10.3934/jcd.2014.1.391
51. Bravo, N., Smith, R.C., Crews, J.: Surrogate model development and feedforward control implementation for PZT bimorph actuators employed for robobee. In: Proc. SPIE, vol. 10165. https://doi.org/10.1117/12.2259948 (2017a)
52. Bravo, N., Smith, R.C., Crews, J.: Data-Driven Model Development and Feedback Control Design for PZT Bimorph Actuators. https://doi.org/10.1115/SMASIS2017-3847 (2017b)
53. Bravo, N., Smith, R.C.: Parameter-dependent surrogate model development for PZT bimorph actuators employed for micro-air vehicles. In: Proc. SPIE, vol. 10968. https://doi.org/10.1117/12.2514246 (2019)
54. Kurdila, A.J., Bobade, P.: Koopman Theory and Linear Approximation Spaces. arXiv:1811.10809 (2018)
55. Hultmann Ayala, H.V., Habineza, D., Rakotondrabe, M., Klein, C.E., Coelho, L.S.: Nonlinear black-box system identification through neural networks of a hysteretic piezoelectric robotic micromanipulator. IFAC-PapersOnLine **48**(28), 409–414 (2015). https://doi.org/10.1016/j.ifacol.2015.12.162
56. Yang, S.M., Lee, G.S.: System identification of smart structures using neural networks. J. Intell. Mater. Syst. Struct. **8**(10), 883–890 (1997). https://doi.org/10.1177/1045389X9700801008
57. Mohammadzaheri, M., Grainger, S., Bazghaleh, M., Yaghmaee, P.: Intelligent modeling of a piezoelectric tube actuator. In: 2012 International Symposium on Innovations in Intelligent Systems and Applications, pp. 1–6. https://doi.org/10.1109/INISTA.2012.6246980 (2012a)
58. Mohammadzaheri, M., Grainger, S., Bazghaleh, M.: A comparative study on the use of black box modelling for piezoelectric actuators. Int. J. Adv. Manuf. Technol. **63**(9), 1247–1255 (2012b). https://doi.org/10.1007/s00170-012-3987-5
59. Yu, S., Alici, G., Shirinzadeh, B., Smith, J.: Sliding mode control of a piezoelectric actuator with neural network compensating rate-dependent hysteresis. In: Proceedings of the 2005 IEEE International Conference on Robotics and Automation, pp. 3641–3645. https://doi.org/10.1109/ROBOT.2005.1570674 (2005)
60. Bobade, P., Majumdar, S., Pereira, S., Kurdila, A.J., Ferris, J.B.: Adaptive estimation for nonlinear systems using reproducing kernel Hilbert spaces. Adv. Comput. Math. **45**(2), 869–896 (2019). https://doi.org/10.1007/s10444-018-9639-z
61. Joshi, G., Chowdhary, G.: Adaptive control using Gaussian-process with model reference generative network. In: 2018 IEEE Conference on Decision and Control (CDC), pp. 237–243. https://doi.org/10.1109/CDC.2018.8619431 (2018)
62. Axelrod, A.M., Kingravi, H.A., Chowdhary, G.V.: Gaussian process based subsumption of a parasitic control component. In: 2015 American Control Conference (ACC), pp 2888–2893. https://doi.org/10.1109/ACC.2015.7171173 (2015)
63. Chowdhary, G., Kingravi, H.A., How, J.P., Vela, P.A.: A Bayesian nonparametric approach to adaptive control using Gaussian processes. In: 52nd IEEE Conference on Decision and Control, pp. 874–879. https://doi.org/10.1109/CDC.2013.6759992 (2013)
64. Maske, H., Kingravi, H.A., Chowdhary, G.: Sensor selection via observability analysis in feature space. In: 2018 Annual American Control Conference (ACC), pp. 1058–1064. https://doi.org/10.23919/ACC.2018.8431625 (2018)
65. Whitman, J., Chowdhary, G.: Learning dynamics across similar spatiotemporally-evolving physical systems. In: Levine, S., Vanhoucke, V., Goldberg, K. (eds.) Proceedings of the 1st Annual Conference on Robot Learning, PMLR, Proceedings of Machine Learning Research, vol. 78, pp. 472–481. http://proceedings.mlr.press/v78/whitman17a.html (2017)
66. Kingravi, H.A., Maske, H., Chowdhary, G.: Kernel controllers: a systems-theoretic approach for data-driven modeling and control of spatiotemporally evolving processes. In: 2015 54th IEEE Conference on Decision and Control (CDC), pp. 7365–7370. https://doi.org/10.1109/CDC.2015.7403382 (2015)
67. Kurdila, A.J., Tarazaga, P.: Vibrations of Linear Piezostructures. Wiley, Hoboken (2018). (in press)
68. Tiersten, H.F.: Linear Piezoelectric Plate Vibrations. Springer, Boston (1969). https://doi.org/10.1007/978-1-4899-6453-3
69. Cottone, F., Gammaitoni, L., Vocca, H., Ferrari, M., Ferrari, V.: Piezoelectric buckled beams for random vibration energy harvesting. Smart Mater. Struct. **21**(3), 35021 (2012). https://doi.org/10.1088/0964-1726/21/3/035021
70. Friswell, M.I., Ali, S.F., Bilgen, O., Adhikari, S., Lees, A.W., Litak, G.: Non-linear piezoelectric vibration energy harvesting from a vertical cantilever beam with tip mass. J. Intell. Mater. Syst. Struct. **23**(13), 1505–1521 (2012). https://doi.org/10.1177/1045389X12455722
71. Rakotondrabe, M., Haddab, Y., Lutz, P.: Quadrilateral modelling and robust control of a nonlinear piezoelectric cantilever. IEEE Trans. Control Syst. Technol. **17**(3), 528–539 (2009). https://doi.org/10.1109/TCST.2008.2001151
72. Aronszajn, N.: Theory of reproducing kernels. Trans. Am. Math. Soc. **68**(3), 337–404 (1950). https://doi.org/10.2307/1990404
73. Berlinet, A., Thomas-Agnan, C.: Reproducing Kernel Hilbert Spaces in Probability and Statistics. Springer, Berlin (2011)
74. Muandet, K., Fukumizu, K., Sriperumbudur, B., Schölkopf, B.: Kernel mean embedding of distributions: a review and beyond. Found. Trends Mach. Learn. **10**(1–2), 1–141 (2017)

75. Pazy, A.: Semigroups of Linear Operators and Applications to Partial Differential Equations, vol. 44. Springer, Berlin (2012)
76. Ioannou, P.A., Sun, J.: Robust Adaptive Control. Dover Publications Inc, New York (1996)
77. Sastry, S., Bodson, M.: Adaptive Control: Stability, Convergence and Robustness. Courier Corporation, North Chelmsford (2011)
78. Narendra, K.S., Annaswamy, A.M.: Stable Adaptive Systems. Courier Corporation, North Chelmsford (2012)
79. Guo, J., Paruchuri, S.T., Kurdila, A.J.: Persistence of excitation in uniformly embedded reproducing kernel Hilbert (RKH) spaces (ACC). In: American Control Conference (2020)
80. Guo, J., Paruchuri, S.T., Kurdila, A.J.: Persistence of excitation in uniformly embedded reproducing kernel Hilbert (RKH) spaces. Syst. Control Lett. (2019)
81. Kurdila, A.J., Guo, J., Paruchuri, S.T., Bobade, P.: Persistence of Excitation in Reproducing Kernel Hilbert Spaces, Positive Limit Sets, and Smooth Manifolds. http://arxiv.org/abs/1909.12274 (2019)
82. Kurdila, A.J., Narcowich, F.J., Ward, J.D.: Persistency of excitation in identification using radial basis function approximants. SIAM J. Control Optim. **33**(2), 625–642 (1995)